Applied Physics Letters

Contact passivation for defect mitigation in multi-dimensional perovskite interfaces

Cite as: Appl. Phys. Lett. **119**, 141602 (2021); https://doi.org/10.1063/5.0061908
Submitted: 30 June 2021 . Accepted: 17 September 2021 . Published Online: 04 October 2021

Sundheep R. and Ankit Jain

AIP Publishing

Applied Physics Letters ARTICLE scitation.org/journal/apl

Contact passivation for defect mitigation in multi-dimensional perovskite interfaces

Cite as: Appl. Phys. Lett. **119**, 141602 (2021); doi: 10.1063/5.0061908
Submitted: 30 June 2021 · Accepted: 17 September 2021 ·
Published Online: 4 October 2021

Sundheep R. and Ankit Jain[a)]

AFFILIATIONS

Mechanical Engineering Department, Indian Institute of Technology, Bombay, India

Note: This paper is part of the APL Special Collection on New Solution-processed Perovskites and Perovskite-inspired Optoelectronic Materials and Devices.
[a)]**Author to whom correspondence should be addressed:** a_jain@iitb.ac.in

ABSTRACT

Multi-dimensional perovskite (MDP) interface consisting of a lower-dimensional (2D) perovskite phase sandwiched between a bulk (3D) perovskite layer and a charge transporting layer is being propounded as a feasible solution for enhancing the stability of perovskite solar cells (PSCs). Here, using first principles-based density functional theory calculations, we study the effect of interface anion engineering on the stability and electronic property of the MDP interfaces. We find that 2D–3D perovskite interfaces are highly stable and are immune to interfacial defect formation. Furthermore, interface chlorination helps in mitigating the deleterious effect of charge localization for antisite defects at these interfaces. For an interface between 2D-perovskite and a charge-extracting TiO_2 layer, we find that interfacial anion engineering is instrumental in alleviating the lattice mismatch induced instability. We propose that opposed to interfacial defects, the hole localization arising due to the presence of interfacial halide at the pristine 2D-TiO_2 interface is the major obstacle that needs to be overcome for achieving a defect immune MDP for realizing a PSC with ultrahigh stability and performance.

The success of hybrid organic–inorganic perovskites as an effective photo-absorber material in thin-film solar cell architecture is attributed to their transcendent electronic properties of strong absorption coefficient, low exciton binding energy, and relatively long carrier diffusion length.[1] These advantages, combined with solution processability of earthly abundant materials, make perovskites a promising contender for future commercial photovoltaic technologies.[2] The performance of solar cells employing perovskite absorber materials demonstrated a significant enhancement from less than 4% in 2011 to 24% in 2020, nearing their benchmark thermodynamic limit.[3] However, their success as a commercial photovoltaic technology is currently hindered by their poor stability and performance degradation originating primarily from atomic defects formed at the material interface between the active perovskite material and the electron extraction layer in the thin film device.[4]

Consequently, different defect passivation approaches have been proposed for interfaces between absorber and electron extraction layers.[5] For instance, (a) an ultrathin PMMA:PCBM mixture was introduced as a passivation layer and resulted in an enhanced open-circuit voltage and fast current/voltage response time,[6] (b) a dual surface modification from $TiCl_4$ treatment and monolayer PC61BM deposition was employed for single-crystalline TiO_2 nanotube arrays based PSCs and resulted in a photoconversion efficiency (PCE) of 19.5%,[7] (c) alkali metals based passivation layers are tested and found to be effective in enhancing the fill factor, reducing the interfacial recombination, and the hysteresis behavior observed in the PSCs.[5] Despite these signs of progress, however, a definite passivation strategy to facilitate the commercialization of perovskite photovoltaic technology remains elusive.

Recently, significant stability enhancements are achieved by introducing 2D counterparts of the 3D perovskite that have better stability under device operation conditions.[8] Here, 3D perovskite refers to a bulk organic inorganic halide perovskite compound adopting a general ABX_3 perovskite structure, while 2D perovskite refers to Ruddlesden popper family of 2D perovskites, which are obtained by cleaving the 3D perovskite along their ⟨100⟩ crystal direction. Grancini *et al.* used 2D perovskite as a buffer layer at the ETL interface and achieved a PCE of 11.2% with stability of more than 10 000 h.[9] Peng *et al.* inserted a fluoroarene based 2D perovskite layer between the absorbing layer and the hole transporting layer to achieve an ultrahydrophobic PSC with efficiency exceeding 22% and enhanced stability under laboratory testing conditions.[10] During MDP interface

fabrication, the natural tendency of the 2D perovskite phase is to grow with the organic cations parallel to the interface.[11] Introducing 2D perovskite with parallel orientation at the hole transport layer/3D perovskite interface was found to retard the charge recombination, thereby enhancing the V_{OC}, without inhibiting the current extraction of the PSCs.[12] Furthermore, double sided 2D perovskite layers was found to provide effective defect passivation at both the electron and hole transport layer/perovskite interface. In spite of the semi-insulating nature of the organic cations, an increase in charge transfer and the fill factor were observed for the double side passivated PSCs compared to unpassivated PSCs resulting in superior PCE.[13,14] Further optimization and fine tuning of the MDP interface require a clear cut understanding of electronic properties arising due to parallel alignment happening at the interface.[15] Interfacial anion engineering and its effect on the electronic properties of the MDP interface has been very rarely explored until date.

The experimental studies carried out to assess the defect dynamics in these materials have pointed out the existence of deep level traps in quasi-2D halide perovskites with an order of magnitude higher defect density than that in 3D perovskites.[16] For 3D perovskites, the energetics of the defect formation, their effect on the electronic properties of the material, and various defect passivation methods are well studied. For 2D perovskites, corresponding studies are limited. Specifically, the influence of interfacial defects on the heterostructure stability and device performance still remains an open question for 2D perovskite based MDP PSCs.

Density Functional Theory (DFT) calculations have been instrumental in the understanding of the defect formation physics at perovskite interfaces. These calculations suggested that (i) the presence of uncoordinated TiO_2 and surface halides promotes the growth of the (110) 3D perovskite structure over TiO_2,[17] (ii) chlorine doping in small amounts is beneficial to the electronic structure, inorganic framework lattice disorder, and cation libration motion of the crystal enabling easy exciton dissociation, and lower charge recombination in perovskite materials,[18] and (iii) vacancy defects at the TiO_2 part of the 3D-TiO_2 interface is detrimental for hole transport and results in enhanced recombination rates, demonstrating the importance of defect-free TiO_2 for achieving a better performing PSC,[19] etc. These theoretical results are experimentally confirmed and resulted in a low temperature, solution-processed, and stable PSC originating from stronger binding of the chlorinated 3D perovskite-TiO_2 interface. The above-mentioned studies employed a heterointerface, which is representative of perovskite-mesoporous/compact TiO_2 interface present in a PSC device demonstrating the validity of the models used in the DFT calculations.[20] Recently, based on DFT calculations, planar SnO_2 was proposed as a better alternative for mesoporous TiO_2 but the performance efficiencies of SnO_2 based devices were found to be lower compared to TiO_2 based devices.[20,21] A DFT calculation guided rational design of defect passivators has helped in optimizing the efficiency of PSCs to 22.6% using naturally abundant molecules.[22]

In this work, we use DFT calculations to study different interfaces in an MDP heterostructure employed in a PSC. In particular, we study the interfacial defect formation at $MAPbI_3$ (methylammonium lead iodide, 3D-perovskite)-$BTAPbI_4$ (butylammonium lead iodide, 2D-perovskite)-TiO_2 (charge selective layer) interface and contrast them with a standard 3D-TiO_2 interface to elucidate the role of MDP interfaces in a PSC device architecture. The effect of different interfacial defects (vacancy, antisite, and substitutional) on the electronic properties of the interfacial MDP is investigated, and the role of chlorine contact passivation in mitigating interface defects is highlighted.

DFT calculations are performed using a Perdew Burkew Ernzerhof generalized gradient exchange correlation functional.[23] All calculations are performed using a plane wave basis set, using projected augmented wave pseudopotential as implemented in Vienna *ab initio* simulation package.[24,25] The plane wave kinetic energy cutoff is fixed at 400 eV, and the van der Waals interactions are modeled using the DFT-D3 method of Grimme.[26] The Brillouin zone is sampled using the Gamma-only wavevector grid, and an electronic convergence criterion of 10^{-5} eV per formula unit is used. The convergence of reported results with electronic wavevector grid is tested on a representative 3D-TiO_2 interface and reported in Table S1. The calculations suggest that the changes in formation energies are less than 0.29 eV/nm^2 in increasing the electronic wavevector grid to $4 \times 4 \times 1$ from $1 \times 1 \times 1$. All geometry optimization and partial density of states (pDOS) calculations are performed without including the spin–orbit coupling. A comparison of pDOS calculated for pristine and defective interfaces with and without SOC given in the supplementary material (Figs. S1–S7) shows that accounting for SOC effects does not lead to marked variation in the defect states. A minimum vacuum of 15 Å is ensured in the direction perpendicular to the interface in all calculations. The heterostructures are created while ensuring minimal lattice mismatch between the interface forming materials. All heterostructures are relaxed to minimize forces to less than 0.05 eV/Å. Previous studies have reported that after relaxation, the in-plane lattice parameters of the 3D-TiO_2 interface are closely related to the lattice parameters of the TiO_2 part of the interface.[19] Hence, for 3D-TiO_2 and 2D-TiO_2 interfaces, the in-plane lattice constants are fixed at that of the TiO_2 layer while for the 2D-3D interface, all lattice degrees (except vacuum) are allowed to change during relaxation.

The 2D-TiO_2 interface is created by modeling the $5 \times 2 \times 1$ (001) $BTAPbI_4$ with the $5 \times 3 \times 2$ (101) TiO_2 surface consisting of a total of 1260 atoms. The 2D–3D interface is formed by modeling the $5 \times 3 \times 2$ (001) $BTAPbI_4$ with $5 \times 3 \times 2$ (001) $MAPbI_3$ with a total of 1350 atoms. Finally, the 3D-TiO_2 interface is modeled as $3 \times 5 \times 3$ (110) $MAPbI_3$ with a $5 \times 3 \times 2$ (101) TiO_2 surface consisting of a total of 900 atoms. The (101) termination of TiO_2 is selected based on previous literature reports suggesting preferential growth of perovskite at the TiO_2 (101) surface.[17] For $MAPbI_3$, tetragonal (110) and (001) surfaces are formed from alternative stacking of charge neutral MAI and PbI_2 layers and are intrinsically more stable compared to other surfaces.[27] Of these, the (110) surface is preferred on TiO_2 due to a better lattice match.[17] Furthermore, depending on the growth conditions, while both MAI and PbI_2 terminations are possible,[28] the MAI surface termination is found to be advantageous for averting carrier trapping happening on the perovskite surface states.[29] As such, all surfaces are created with MAI termination in this study (Fig. 1).

To study the effect of Cl atoms in contact passivation, all I atoms at the interface are replaced with Cl atoms. The antisite defects (AD) are created at interfaces by randomly exchanging the positions of I/Cl atom with the Pb atom at the interface. Similarly, vacancy defects (VD) are created by randomly removing the desired species atom from the interface. The organic layer termination adopted in the case of 2D perovskites results in a crystal structure where the longer butyl ammonium cations are present at the interface with the neutral PbI_2

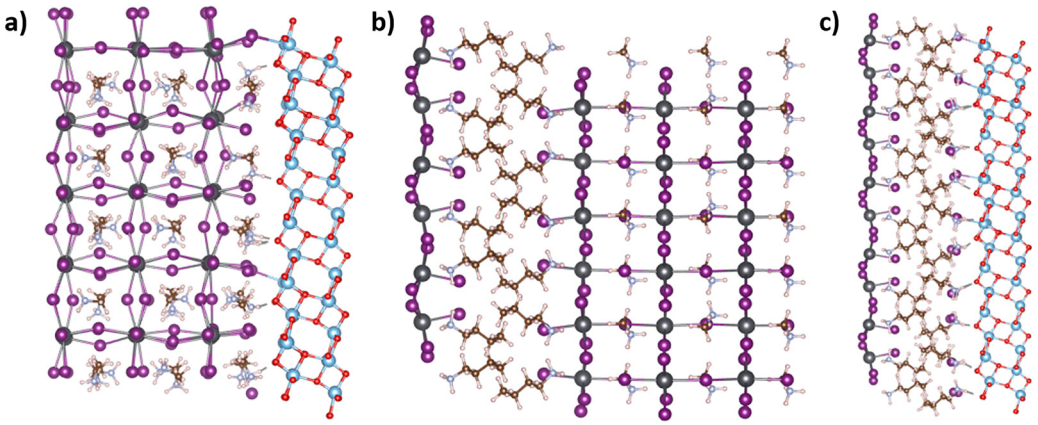

FIG. 1. The three different interfaces employed in the study, (a) 110 $MAPbI_3$–101 TiO_2, (b) 001 $BTAPbI_4$–001 $MAPbI_3$, and (c) 001 $BTAPbI_4$–101 TiO_2 interface.

layer situated farther away from the interface, which limits the creation of interfacial AD. To study the effect of AD like defects for a 2D-TiO_2 interface, we created substitutional defects (SD), and they differ from AD in their absence of a charge compensating halide ion near the SD Pb atom. In the case of the 2D-TiO_2 interface, SD are created by replacing a single I/Cl atom at the interface with a Pb atom. Consequently, VD/SD are charged defects, and AD are charge-neutral defects. Three random defect configurations are created for each defect, and the relative atomic arrangements are maintained between chlorinated and non-chlorinated interfaces.

The formation energies of the pristine interfaces are obtained as

$$E_{FE} = \frac{E_{Interface} - E_{surface1} - E_{surface2}}{area}, \quad (1)$$

where E_{FE} is the formation energy of the pristine interface, $E_{Interface}$ is the relaxed energy of the interface, $E_{surface1}$ and $E_{surface2}$ are the relaxed energy of first and second molecular material surfaces, which makeup the interface, respectively, and the area is the total surface area of the interface supercell. Defect formation energies (FEs) of chlorinated and non-chlorinated interfaces are calculated by subtracting the relaxed energies of defective supercells from their pristine supercell counterparts. Out of the three defect configurations, the defects having the lowest formation energy (most stable) values are used for analysis. pDOS is plotted to identify the defects with mid-bandgap electronic states. Wavefunction visualization happening at the defect position is employed to understand the charge carrier localization at the defective interfaces. The effect of defects on the electronic properties is to transform the extended energy eigenstates of perfectly ordered potential into localized states.[30] The second moment of the wave-function probability amplitude, i.e., the inverse participation ratio, can be used as a criterion to distinguish localized and extended states. The lower limit of IPR corresponds to a completely delocalized state, while an increase in IPR value is indicative of the localization happening at the defective site.[31] The inverse participation ratio (IPR) of the defective states is calculated to quantify the extent of wavefunction localization.[32]

We start our analysis by evaluating the stability of pristine non-chlorinated and chlorinated 3D-TiO_2, 2D-TiO_2, and 2D–3D interfaces. The corresponding FEs are reported in Table I. We find that for non-chlorinated interfaces, the interface formation between 2D–3D perovskite is highly favorable with FE of −3.1 eV/nm^2. In comparison, the interfaces of 2D/3D perovskites with TiO_2 are more rigid, resulting in lower FEs. Among these two interfaces, 2D-TiO_2 interface is found to be less stable compared to the other interfaces due to the higher lattice mismatch present at the interface. With chlorination, 2D-TiO_2 becomes more stable due to the enhanced binding as reflected in the reduction in the interlayer distance from 2.978 Å for the non-chlorinated 2D-TiO_2 interface to 2.409 Å for the chlorinated interface. The effect of chlorine/fluorine incorporation on the microstructure evolution, perovskite thin film formation process, and the enhanced stability arising thereof has been reported previously.[33,34] Consistent with our findings, notable enhancement in carrier lifetime and diffusion length was also observed indicating the positive influence of chlorination on the electronic properties of perovskite thin films.[36–38] With their superior hydrophobicity and possibility of interactions with a wide range of atoms/molecules, fluorine can act as a typical passivation molecule for PSCs.[34] However, since the mechanism of defect passivation and enhancement in interfacial stability was found to be similar after chlorine/fluorine passivation at the 3D-TiO_2 interface, we

TABLE I. Lattice mismatch and formation energy values of 3D-TiO_2 and MDP interface for chlorinated and non-chlorinated cases. The values are obtained with corresponding free surfaces as energy reference.

	Lattice mismatch along the x-direction and y-direction (%)	Formation energy (eV/nm^2)	
		Non-chlorinated interface	Chlorinated interface
$MAPbI_3$-TiO_2 (3D-TiO_2)	0.26 0.62	−1.90	−1.60
$BTAPbI_4$-TiO_2 (2D-TiO_2)	0.91 3.44	−1.44	−1.91
$BTAPbI_4$-$MAPbI_3$ (2D−3D)	2.28 1.05	−3.06	−3.01

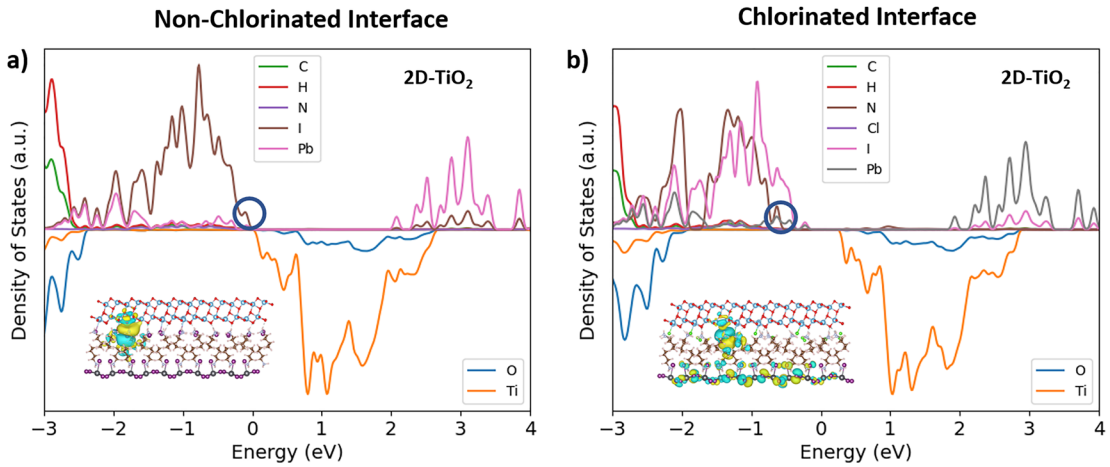

FIG. 2. pDOS plots of the pristine (a) non-chlorinated 2D-TiO_2 and (b) chlorinated 2D-TiO_2 interface. (The inset image shows the wavefunction localization happening around the interfacial halide atoms.)

restrict ourselves to interfacial chlorine passivation in this study.[35] The inherent stability of the 2D-3D interfaces and the enhancement in stability of lattice mismatched 2D-TiO_2 interface after chlorination with respect to the prototypical 3D-TiO_2 interface illustrate the synergetic role of 2D perovskites and interfacial chlorination to enhance the stability while simultaneously reducing the defect density at the interface.

Off the two interfaces present in an MDP heterostructure, the 2D-TiO_2 interface represents an interesting case as the presence of unsaturated halide atoms at the organic cation terminated interface of 2D perovskites acts as hole localization centers.[39] The instantaneous charge (both conduction and valence band) localization was found to result in frequent opening of a non-adiabatic channel through which photogenerated carriers can recombine non-radiatively.[40] Moreover, hole localization at the electron selective layer perovskite interface can modify the charge extraction in the device by generating an electric field, which can lead to current–voltage hysteresis in PSCs.[41] Hence, further theoretical and experimental studies are required to analyze in detail the influence of a hole localizing halide atom near the 2D-TiO_2 interface. The wavefunctions corresponding to these states are plotted in Figs. 2(a) and 2(b), respectively, for non-chlorinated and chlorinated interfaces. The strong charge localization is observed for the non-chlorinated case with an IPR of 311 [Fig. 2(a)]. With chlorination, the localization persists and IPR increases to 515, thereby indicating that these states are deleterious for charge extraction at the 2D-TiO_2 interface. We note that the localization at the bottom of the chlorinated interface [Fig. 2(b)] arises due to the spurious effects resulting from the limited thickness of the 2D perovskite present at the interface. The adoption of thin 2D perovskite layer was necessitated due to the large supercell employed in the study.

Moving further, now that we know that 2D–3D is more stable compared to 3D-TiO_2 and chlorine-passivation helps one to increase the MDP interface stability, we next focus our attention on interface defects. The interfacial defects can hinder the charge extraction by acting as a trap, thereby reducing the device performance. The FEs of different interfacial defects for both chlorinated and non-chlorinated interfaces are reported in Table II. For charge-balanced AD, the reported FEs are with respect to pristine interface and, thus, can be compared between different interfaces/passivations. For VD/SD defects, the FEs do not include the contribution from defect-species chemical potential, and these numbers should only be compared for the same involved defect-species.

We start by investigating charge-neutral AD defects at the 3D-TiO_2 and 2D–3D interfaces. The FE values reported in Table II suggest a high probability of defect formation at the 3D-TiO_2 interface. The high-density of ADs in the case of the 3D-TiO_2 interface is reduced on Cl-passivation (as indicated by an increase in FE) because of the stronger binding happening at the perovskite TiO_2 interface. In comparison, AD are much less likely to form at the 2D–3D interface and have FE of more than 1.63 eV. The better crystallographic connectivity existing between the different perovskite phases results in higher defect FEs at the 2D–3D interface. After chlorination, at the 2D–3D interface, FE of the AD decreases but higher FE values compared to the 3D-

TABLE II. Formation energies of antisite, vacancy, and substitutional defects formed at the 3D-TiO_2, 2D-TiO_2, and 2D–3D non-chlorinated and chlorinated interfaces. Note that for the charged VD and SD defects, the reported values are without including the effect of chemical potential of defect-species.

	Non-chlorinated interface (eV)	Chlorinated interface (eV)
AD		
3D-TiO_2	0.14	0.58
2D- 3D	1.63	0.70
VD		
3D-TiO_2	1.52	3.34
2D- TiO_2	1.77	3.31
2D- 3D	3.70	4.75
SD		
3D-TiO_2	−2.82	−1.73
2D-TiO_2	−2.00	−0.64
2D-3D	1.04	2.13

TiO_2 interface indicate that the defect density will be lower at the 2D–3D interface.[42] This trend of reduced defect density and its advantageous impact on device performance is also observed in experiments involving chlorine passivated PSCs. Compared to the non-passivated interface, the Cl-passivated device resulted in 20.36% efficiency and retaining 94% of its initial stability after testing at maximum power point for more than 600 h.[43]

The pDOS and selected wavefunctions of AD at the 2D–3D and 3D-TiO_2 interfaces are plotted in Figs. 3(a) and 3(c). As observed, AD at the non-chlorinated and chlorinated 3D-TiO_2 interface do not lead to the formation of any mid-bandgap state. The absence of mid-bandgap states in the case of AD can be explained by the local coordination of the interfacial Pb atom. The coordination requirements of the antisite Pb atom are satisfied by three halide atoms surrounding the Pb atom and an oxygen atom at the TiO_2 interface. For 2D–3D, the number of I atoms necessary to fulfill the coordination requirements of antisite Pb atom is insufficient, resulting in an under coordinated Pb atom at the interface. The presence of this under coordinated Pb atom leads to the formation of a mid-bandgap state [Fig. 3(b)] and a highly localized AD in the case of the non-chlorinated 2D–3D interface (IPR value of 140). With chlorination, the FE for AD decreased suggesting a higher probability of these defects at chlorinated 2D–3D interfaces, but the IPR value also decreased, thereby suggesting successful delocalization of AD defects on chlorination (IPR value decreases from 140 for non-chlorinated interface to 42 for the chlorinated interface). As such, while AD are quite likely to form at the 3D-TiO_2 interface, they do not lead to the formation of a mid-bandgap state or a charge carrier localizing defect. In contrast, while AD act as a trap in the case of non-chlorinated 2D–3D interface, the FE values are high, indicating the low density of these defects. Furthermore, with chlorination, while FE remains fairly positive, the charge density delocalizes. The effect of interfacial AD on the performance of an MDP solar cell is, therefore, expected to be minimal.

For the charged VD and SD defects, the FE reported in Table II does not account for chemical potentials of involved species, which depend on the relative concentration of different reactants under the growth conditions. As such, while the reported numbers are not FE and are not comparable between Cl and non-Cl interfaces, these numbers, nevertheless, provide an estimate for the relative stability of defects at different interfaces under the same growth conditions.

For interfacial VD, the propensity of defect formation at 2D-TiO_2 and 2D–3D interfaces is much smaller than the corresponding

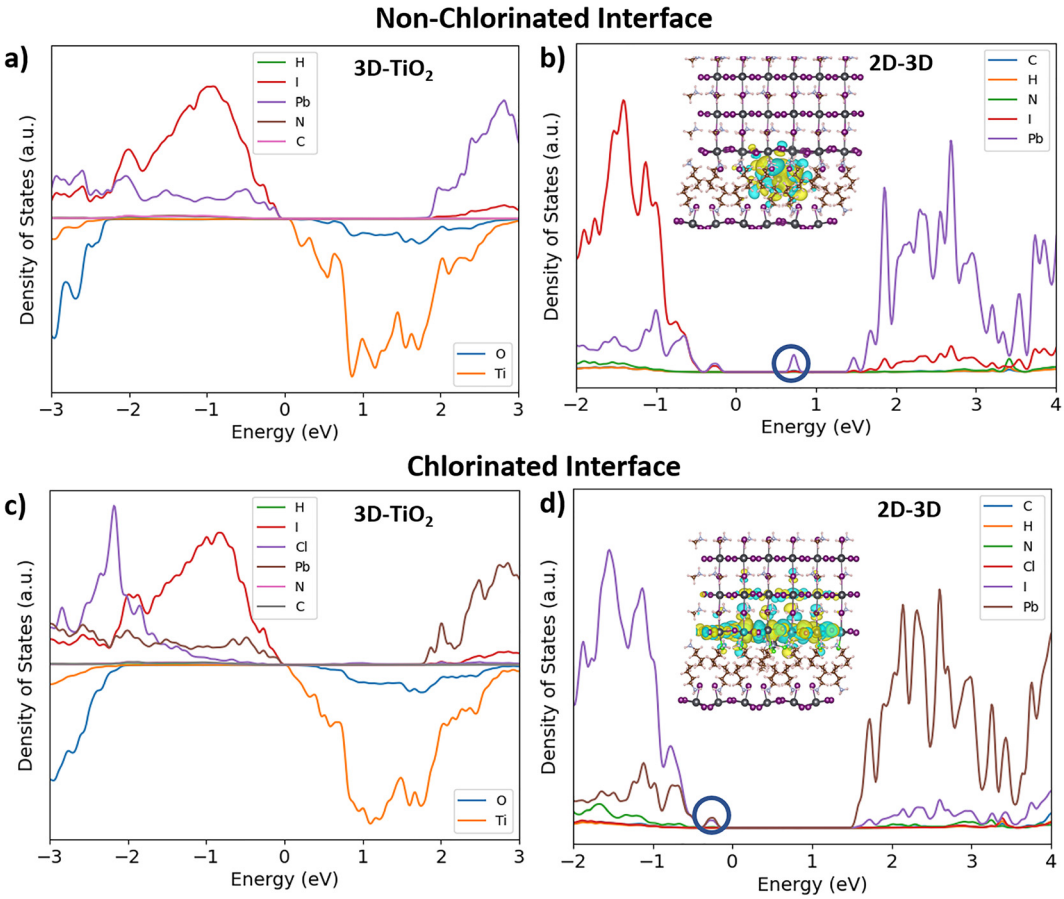

FIG. 3. pDOS plots of the antisite defects formed at non-chlorinated (a) 3D-TiO_2, (b) 2D–3D interface and chlorinated, (c) 3D-TiO_2, (d) 2D–3D interface, respectively. (The inset images show the wavefunction visualization of mid-bandgap state forming interface defect.)

3D-TiO_2 interfaces. In particular, the interfaces between 2D and 3D are nearly perfect, and the relative FE for VD at 2D–3D interface is 1 eV or larger than the corresponding 3D-TiO_2 interface. VD do not exhibit any mid-bandgap states and are highly delocalized in the case of 3D-TiO_2 and 2D–3D interfaces, and as such have little impact on the PSC performance [Figs. 4(a) and 4(d) and 4(c) and 4(f)]. For the 2D-TiO_2 interface, a high degree of wavefunction localization is observed for both non-chlorinated and chlorinated interfaces [an IPR value of 312 for the non-chlorinated and 556 for the chlorinated interface as seen in Figs. 4(b) and 4(e)]. The relative FE for VD defects at 2D-TiO_2 interface remains similar to that of the corresponding 3D-TiO_2 interface.

Similar to the behavior observed in VD, the MDP interfaces are much more resilient to the formation of SD as indicated by their relatively large FE values compared to the non-chlorinated 3D-TiO_2 interface. After chlorination, the relative FEs of SD at the MDP interfaces are 1 eV larger compared to the corresponding 3D-TiO_2 interface. The presence of an under coordinated Pb atom in the case of SD at the 3D-TiO_2 interface leads to the formation of a shallow trap near the CBM edge [Fig. 5(a)]. The wavefunction visualization indicates that this shallow defect does not lead to considerable charge carrier localization. After chlorination, these shallow traps disappear, highlighting the effectiveness of interface chlorination in SD defect passivation at the 3D-TiO_2 interface [Fig. 5(d)]. The SD at the 2D-TiO_2 interface does not lead to the formation of a mid-bandgap state. The wavefunction localization observed at the interface arises due to the existence of unsaturated covalent bonds present on the interfacial halide atoms [Fig. 5(b)]. Upon chlorine passivation, the charge accumulation at the interface is found to increase in the case of SD [Fig. 5(e)] as can be seen from the increasing IPR values (from 311 for the non-chlorinated interface to 642 for the chlorinated interface). The trend of increasing IPR values after chlorination and similarity of the IPR values at the pristine and defective 2D-TiO_2 interface points to the fact that chlorination is not an effective strategy for mitigating the charge carrier localization inherently present at the 2D-TiO_2 interface. For the 2D–3D interface, SD present at the non-chlorinated interface leads to the formation of a mid-bandgap state [Fig. 5(c)] with a high degree of wavefunction localization. Compared to 2D/3D-TiO_2 interfaces, under coordinated Pb atoms are present on either side at the 2D–3D interface, and due to the strong covalent nature of the Pb atom, they result in the formation of a Pb dimer.[44,45] On chlorination, the IPR values remain unchanged (73 for non-chlorinated and 72 for chlorinated interface), indicating that once these defects are formed, chlorine passivation is not much effective. Nevertheless, the relative FE of these defects are more than 2.5 eV larger than the corresponding 3D-TiO_2 interface, thereby suggesting their low densities at the 2D–3D interface compared to that at the 3D-TiO_2 interface.

The seminal work in the field of 2D/3D interfaces was carried out by Grancini *et al.* where the authors demonstrated one-year stable 2D/3D perovskite solar cell based on $MAPbI_3$ with 14.6% efficiency. This 2D/3D configuration by Grancini *et al.* remains the most stable PSC reported until date.[9] This motivated us to study the MDP interface created with $MAPbI_3$, which can act as a prototype for other members of the perovskite family. Recently, $FAPbI_3$ and mixed cation perovskite

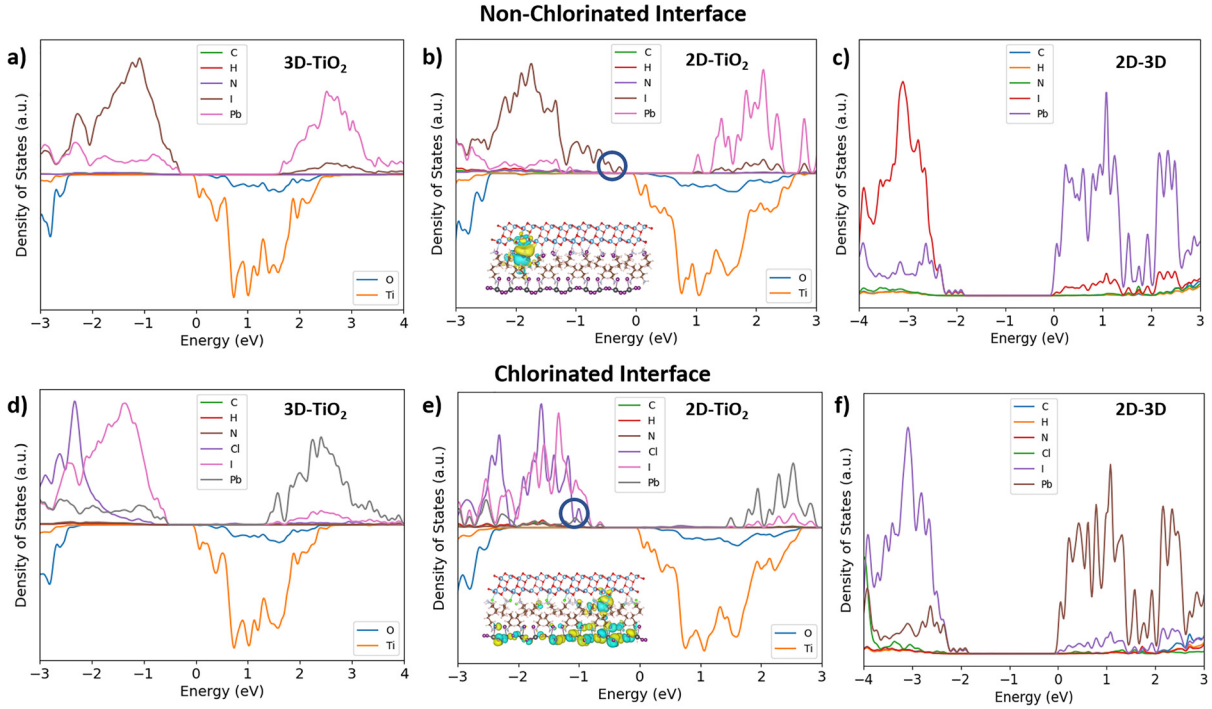

FIG. 4. pDOS plots of the vacancy defects formed at non-chlorinated (a) 3D-TiO_2, (b) 2D-TiO_2, (c) 2D-3D interface and chlorinated (d) 3D-TiO_2, (e) 2D-TiO_2, and (f) 2D-3D interface, respectively. (The inset images show the wavefunction visualization of the mid-bandgap state forming interface defect.)

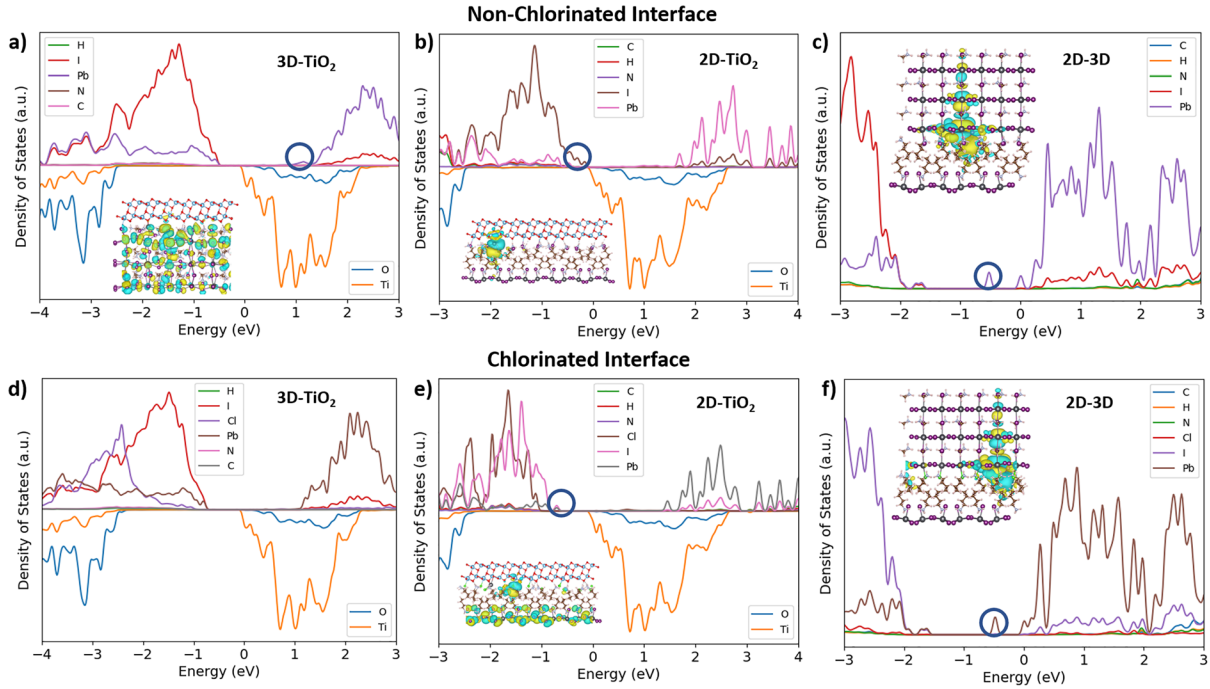

FIG. 5. pDOS plot of substitutional defects formed at non-chlorinated (a) 3D-TiO_2, (b) 2D-TiO_2, and (c) 2D–3D interface and chlorinated (d) 3D-TiO_2, (e) 2D-TiO_2, and (f) 2D–3D interfaces. (The inset image shows the wavefunction localization happening at the defect positions.)

based MDP have been proposed as a superior alternative to replace $MAPbI_3$ in PSCs due to their enhanced thermal stability and favorable bandgap.[46,47] Adopting a similar methodology used in our study could be beneficial in designing $FAPbI_3$ based MDP interface with enhanced stability and defect passivation.

In summary, we have studied the effect of interfacial chlorination on the stability and defect remediation of an MDP interface. The results show that of the two interfaces present in an MDP architecture, the 2D-3D perovskite interface is inherently stable due to better crystallographic connectivity. The charge-neutral AD leads to the formation of mid-bandgap states with a high degree of charge carrier localization at the 2D–3D interface. Interfacial chlorination can be effectively used to reduce the probability of defect formation while simultaneously delocalizing these charge carriers. The introduction of smaller chlorine anions at the interface was found to be seminal in the stability enhancement of the pristine 2D-TiO_2 interface part of the MDP. Charged VD and AD do not lead to the formation of any mid-bandgap state at the 2D-TiO_2 interface but are highly prone to carrier localization due to the presence of interfacial halide atoms. Thus, devising an experimental synthesis/interface modification method to counterbalance the hole localization happening at the 2D-TiO_2 interface will be crucial in realizing a highly stable MDP interface, which will be a critical step forward regarding the commercialization of perovskite photovoltaics.

See the supplementary material for the k-point convergence calculations, density of state plots after taking into consideration the spin–orbit coupling effect, and the optimized interface structure with different defect geometry.

DATA AVAILABILITY

The data that support the findings of this study are available within the article and its supplementary material.

REFERENCES

[1]W. Li, Z. Wang, F. Deschler, S. Gao, R. H. Friend, and A. K. Cheetham, Nat. Rev. Mater. **2**, 16099 (2017).
[2]P. K. Nayak, S. Mahesh, H. J. Snaith, and D. Cahen, Nat. Rev. Mater. **4**, 269 (2019).
[3]M. Vasilopoulou, A. Fakharuddin, and A. G. Coutsolelos, Chem. Soc. Rev. **49**, 4496 (2020).
[4]K. Lim, S. G. Ji, J. Y. Kim, and T. Lee, Small Methods **4**, 2000065 (2020).
[5]J. Kim, A. Ho-Baillie, and S. Huang, Sol. RRL **3**, 1800302 (2019).
[6]J. Peng, Y. Wu, W. Ye, D. A. Jacobs, H. Shen, X. Fu, Y. Wan, T. Duong, N. Wu, C. Barugkin, H. T. Nguyen, D. Zhong, J. Li, T. Lu, Y. Liu, M. N. Lockrey, K. J. Weber, K. R. Catchpole, and T. P. White, Energy Environ. Sci. **10**, 1792 (2017).
[7]F. Shahvaranfard, M. Altomare, Y. Hou, S. Hejazi, W. Meng, B. Osuagwu, N. Li, C. J. Brabec, and P. Schmuki, Adv. Funct. Mater. **30**, 1909738 (2020).
[8]A. Krishna, S. Gottis, M. K. Nazeeruddin, and F. Sauvage, Adv. Funct. Mater. **29**, 1806482 (2019).
[9]G. Grancini, C. Roldán-Carmona, I. Zimmermann, E. Mosconi, X. Lee, D. Martineau, S. Narbey, F. Oswald, F. De Angelis, M. Graetzel, and M. K. Nazeeruddin, Nat. Commun. **8**, 15684 (2017).
[10]Y. Liu, S. Akin, L. Pan, R. Uchida, N. Arora, J. V. Milić, A. Hinderhofer, F. Schreiber, A. R. Uhl, S. M. Zakeeruddin, A. Hagfeldt, M. Ibrahim Dar, and M. Grätzel, Sci. Adv. **5**, eaaw2543 (2019).
[11]P. Liu, N. Han, W. Wang, R. Ran, W. Zhou, and Z. Shao, Adv. Mater. **33**, 2002582 (2021).
[12]M. E. F. Bouduban, V. I. E. Queloz, V. M. Caselli, K. T. Cho, A. R. Kirmani, S. Paek, C. Roldan-Carmona, L. J. Richter, J. E. Moser, T. J. Savenije, M. K. Nazeeruddin, and G. Grancini, J. Phys. Chem. Lett. **10**, 5713 (2019).

[13]M. A. Mahmud, T. Duong, Y. Yin, H. T. Pham, D. Walter, J. Peng, Y. Wu, L. Li, H. Shen, N. Wu, N. Mozaffari, G. Andersson, K. R. Catchpole, K. J. Weber, and T. P. White, Adv. Funct. Mater. **30**, 1907962 (2020).
[14]M. A. Mahmud, T. Duong, Y. Yin, J. Peng, Y. Wu, T. Lu, H. T. Pham, H. Shen, D. Walter, H. T. Nguyen, N. Mozaffari, G. D. Tabi, Y. Liu, G. Andersson, K. R. Catchpole, K. J. Weber, and T. P. White, Small **16**, 2005022 (2020).
[15]R. Quintero-Bermudez, A. H. Proppe, A. Mahata, P. Todorović, S. O. Kelley, F. De Angelis, and E. H. Sargent, J. Am. Chem. Soc. **141**, 13459 (2019).
[16]N. Liu, P. Liu, H. Zhou, Y. Bai, and Q. Chen, J. Phys. Chem. Lett. **11**, 3521 (2020).
[17]E. Mosconi, E. Ronca, and F. De Angelis, J. Phys. Chem. Lett. **5**, 2619 (2014).
[18]C. Quarti, E. Mosconi, P. Umari, and F. De Angelis, Inorg. Chem. **56**, 74 (2017).
[19]J. Haruyama, K. Sodeyama, I. Hamada, L. Han, and Y. Tateyama, J. Phys. Chem. Lett. **8**, 5840 (2017).
[20]J. Kim, K. S. Kim, and C. W. Myung, npj Comput. Mater. **6**, 100 (2020).
[21]Q. Lian, M. Z. Mokhtar, D. Lu, M. Zhu, J. Jacobs, A. B. Foster, A. G. Thomas, B. F. Spencer, S. Wu, C. Liu, N. W. Hodson, B. Smith, A. Alkaltham, O. M. Alkhudhari, T. Watson, and B. R. Saunders, ACS Appl. Mater. Interfaces **12**, 18578 (2020).
[22]R. Wang, J. Xue, K. L. Wang, Z. K. Wang, Y. Luo, D. Fenning, G. Xu, S. Nuryyeva, T. Huang, Y. Zhao, J. L. Yang, J. Zhu, M. Wang, S. Tan, I. Yavuz, K. N. Houk, and Y. Yang, Science **366**, 1509 (2019).
[23]J. P. Perdew, K. Burke, and M. Ernzerhof, Phys. Rev. Lett. **77**, 3865 (1996).
[24]G. Kresse and J. Furthmu, Phys. Rev. B **54**, 11169 (1996).
[25]P. E. Blochl, Phys. Rev. B **50**, 17953 (1994).
[26]S. Grimme, J. Comput. Chem. **27**, 1787 (2006).
[27]J. Haruyama, K. Sodeyama, L. Han, and Y. Tateyama, J. Phys. Chem. Lett. **5**, 2903 (2014).
[28]E. Mosconi, G. Grancini, C. Roldán-Carmona, P. Gratia, I. Zimmermann, M. K. Nazeeruddin, and F. De Angelis, Chem. Mater. **28**, 3612 (2016).
[29]H. Uratani and K. Yamashita, J. Phys. Chem. Lett. **8**, 742 (2017).
[30]S. Ashhab, O. Voznyy, S. Hoogland, E. H. Sargent, and M. E. Madjet, Sci. Rep. **7**, 8902 (2017).
[31]C. Zheng, O. Rubel, M. Kepenekian, X. Rocquefelte, and C. Katan, J. Chem. Phys. **151**, 234704 (2019).
[32]M. Imran, L. Peng, A. Pianetti, V. Pinchetti, J. Ramade, J. Zito, F. Di Stasio, J. Buha, S. Toso, J. Song, I. Infante, S. Bals, and S. Brovelli, J. Am. Chem. Soc. **143**, 1435 (2021).
[33]B. Lee, T. Hwang, S. Lee, B. Shin, and B. Park, Sci. Rep. **9**, 4803 (2019).
[34]N. A. N. Ouedraogo, H. Yan, C. B. Han, and Y. Zhang, Small **17**, 2004081 (2021).
[35]B. M. Lefler, S. J. May, and A. T. Fafarman, Phys. Rev. Mater. **4**, 120301 (2020).
[36]J. Chae, Q. Dong, J. Huang, and A. Centrone, Nano Lett. **15**, 8114 (2015).
[37]H. C. Liao, P. Guo, C. P. Hsu, M. Lin, B. Wang, L. Zeng, W. Huang, C. M. M. Soe, W. F. Su, M. J. Bedzyk, M. R. Wasielewski, A. Facchetti, R. P. H. Chang, M. G. Kanatzidis, and T. J. Marks, Adv. Energy Mater. **7**, 1601660 (2017).
[38]S. T. Williams, F. Zuo, C. C. Chueh, C. Y. Liao, P. W. Liang, and A. K. Y. Jen, ACS Nano **8**, 10640 (2014).
[39]Z. Zhang, W. H. Fang, R. Long, and O. V. Prezhdo, J. Am. Chem. Soc. **141**, 15557 (2019).
[40]W. Li, R. Long, J. Tang, and O. V. Prezhdo, J. Phys. Chem. Lett. **10**, 3788 (2019).
[41]S. A. L. Weber, I. M. Hermes, S. H. Turren-Cruz, C. Gort, V. W. Bergmann, L. Gilson, A. Hagfeldt, M. Graetzel, W. Tress, and R. Berger, Energy Environ. Sci. **11**, 2404 (2018).
[42]Z. Wang, Q. Lin, F. P. Chmiel, N. Sakai, L. M. Herz, and H. J. Snaith, Nat. Energy **2**, 17135 (2017).
[43]Y. Wu, X. Li, S. Fu, L. Wan, and J. Fang, J. Mater. Chem. A **7**, 8078 (2019).
[44]Z. Zhang, L. Qiao, C. Mora-Perez, R. Long, and O. V. Prezhdo, J. Chem. Phys. **152**, 064707 (2020).
[45]M. L. Agiorgousis, Y. Sun, H. Zeng, and S. Zhang, J. Am. Chem. Soc. **136**, 14570 (2014).
[46]J. Jeong, M. Kim, J. Seo, H. Lu, P. Ahlawat, A. Mishra, Y. Yang, M. A. Hope, F. T. Eickemeyer, M. Kim, Y. J. Yoon, I. W. Choi, B. P. Darwich, S. J. Choi, Y. Jo, J. H. Lee, B. Walker, S. M. Zakeeruddin, L. Emsley, U. Rothlisberger, A. Hagfeldt, D. S. Kim, M. Grätzel, and J. Y. Kim, Nature **592**, 381 (2021).
[47]Y. W. Jang, S. Lee, K. M. Yeom, K. Jeong, K. Choi, M. Choi, and J. H. Noh, Nat. Energy **6**, 63 (2021).